ACS APPLIED MATERIALS & INTERFACES

Research Article

Cite This: ACS Appl. Mater. Interfaces 2018, 10, 21173−21183

www.acsami.org

Microdevice Platform for Continuous Measurement of Contractility, Beating Rate, and Beating Rhythm of Human-Induced Pluripotent Stem Cell-Cardiomyocytes inside a Controlled Incubator Environment

Li Wang,[†,⊥] Wenkun Dou,[†,⊥] Manpreet Malhi,[‡] Min Zhu,[†] Haijiao Liu,[†,§] Julia Plakhotnik,[‡] Zhensong Xu,[†] Qili Zhao,[†] Jun Chen,[†] Siyu Chen,[†] Robert Hamilton,[‡] Craig A. Simmons,[*,†,§] Jason T. Maynes,[*,‡] and Yu Sun[*,†,§,∥]

[†]Department of Mechanical and Industrial Engineering, University of Toronto, Toronto ON M5S 3G8, Canada

[‡]Hospital for Sick Children, Toronto ON M5G 1X8, Canada

[§]Institute of Biomaterials and Biomedical Engineering, University of Toronto, Toronto ON M5S 3G9, Canada

[∥]Department of Electrical and Computer Engineering, University of Toronto, Toronto ON M5S 3G4, Canada

Supporting Information

ABSTRACT: The heart completes a complex set of tasks, including the initiation or propagation of an electrical signal with regularity (proper heart rate and rhythm) and generating sufficient force of contraction (contractility). Probing mechanisms of heart diseases and quantifying drug efficacies demand a platform that is capable of continuous operation inside a cell incubator for long-term measurement of cardiomyocyte (CM) monolayers. Here, we report a microdevice array that is capable of performing continuous, long-term (14 days) measurement of contractility, beating rate, and beating rhythm in a monolayer of human-induced pluripotent stem cell-CMs (hiPSC-CMs). The device consists of a deformable membrane with embedded carbon nanotube (CNT)-based strain sensors. Contraction of the hiPSC-CMs seeded on the membrane induces electrical resistance change of the CNT strain sensor. Continuously reading the sensor signals revealed that hiPSC-CMs started to beat from day 2 and plateaued on day 5. Average contractile stress generated by a monolayer of hiPSC-CMs was determined to be 2.34 ± 0.041 kPa with a beating rate of 1.17 ± 0.068 Hz. The device arrays were also used to perform comprehensive measurement of the beating rate, rhythm, and contractility of the hiPSC-CMs and quantify the cell responses to different concentrations of agonists and antagonists, which altered the average contractile stress to the range of 1.15 ± 0.13 to 3.96 ± 0.53 kPa. The continuous measurement capability of the device arrays also enabled the generation of Poincaré plots for revealing subtle changes in the beating rhythm of hiPSC-CMs under different drug treatments.

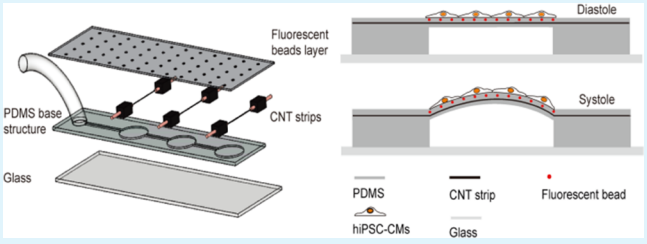

KEYWORDS: *microdevice array, carbon nanotube, continuous measurement, contractile stress, beating rate, beating rhythm, hiPS-cardiomyocytes*

1. INTRODUCTION

Dysfunctions of the human heart, either inherited (e.g., congenital heart disease) or acquired (e.g., cardiac failure), are a major threat to health across the world, leading to 31% of all global deaths.[1] State-of-the-art drug screening for heart disease uses cardiomyocytes (CM) of animals or the Langendorff heart model.[2] However, these models rely on the use of nonhuman tissue or cells to circumvent invasive clinical biopsy procedures, limiting the translation and applicability to human biology. Recent breakthroughs in human-induced pluripotent stem cells (hiPSCs)[3] have made human disease-specific CMs available for screening drugs and elucidating the mechanisms of specific cardiac diseases.

Mechanical forces strongly affect many cellular processes.[4] For CMs, one of the most important mechanical characteristics is their intrinsic ability to produce contractility. The force of this contraction is responsible for pumping adequate oxygen-rich blood from the heart to other organs and tissues.[5] The contraction of CMs is associated with the calcium regulatory proteins,[6] such as the sodium−calcium exchanger and the L-type calcium channel (LTCC). These transmembrane proteins regulate the calcium influx, which is initiated by electrical signaling from the neighboring cells via gap junctions.[7] With the

Received: April 3, 2018
Accepted: June 6, 2018
Published: June 6, 2018

DOI: 10.1021/acsami.8b05407
ACS Appl. Mater. Interfaces 2018, 10, 21173−21183

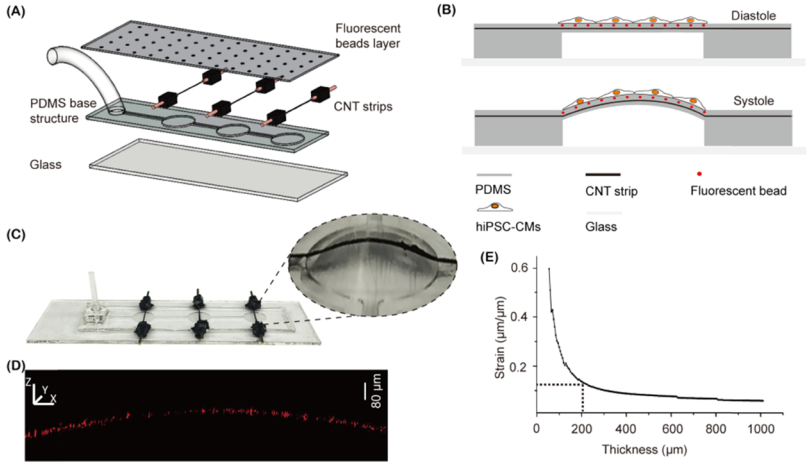

Figure 1. PDMS−CNT devices for the measurement of cardiac contractility. (A) Schematic diagram of PDMS−CNT devices. Screen-printed CNT stripes are sandwiched between two PDMS layers. Fluorescent beads are embedded in the top PDMS layer. (B) Schematic diagram illustrating membrane deflection induced by diastole and systole of monolayer hiPSC-CMs. (C) A completed PDMS−CNT device array including an inlet, CNT stripe, PDMS membrane, connectors, and microchannel. Each array contains three wells. The inset shows bright field under 16.7 kPa. (D) Confocal microscopy images showing membrane budging under 16.7 kPa. (E) Simulation results of membrane maximal strain vs different membrane thicknesses under the bulging pressure of 3.43 kPa. For the PDMS membrane of 200 μm thickness, strain is 0.14.

calcium influx, the thick and thin protein filaments of the sarcomere (the force-generating unit of CMs) slide with each other to produce contraction. To accomplish the vital function, each CM should act synergistically to keep the heart beating rate constant, rhythm consistent, and contractility strong. Thus, the ability to quantify CMs' contractility, beating rate, and beating rhythm is necessary for probing the mechanism of heart disease and quantifying drug efficacies.

Several techniques have been developed for measuring the contractile stress/force of CMs. Table S1 (Supporting Information) summarizes the existing techniques and their working principles. Since 1984, electrical impedance measurement using microelectrode arrays has been used to monitor cell behavior such as growth and spreading.[8] Recently, there have been attempts to utilize impedance signal changes to indicate CMs' contractility.[9,10] Although impedance measurement has inherent capabilities for measuring the beating rate of CMs, direct correlations between the impedance change and contractile stress generated by CMs remain elusive.

For direct contractility measurement, microcantilevers were developed[11,12] where the deflection of the cantilever caused by CM contraction was measured by detecting the reflection angle change of a laser beam shed onto the backside of the cantilever. Heat generated by laser irradiation in microcantilever measurement can cause undesired changes in cell metabolism.[13,14] Existing laser-based cantilevers also require devices with cells cultured on them to be moved in and out of cell incubators for performing each measurement. This is undesired because CMs' contractility, beating rate, and beating rhythm are highly sensitive to environmental parameters such as temperature and concentration of CO_2.[15−17] Laser-based cantilevers fully integrated with measurement components that can achieve long-term, continuous monitoring of CM behaviors remain to be developed.

Piezoresistive cantilevers have recently been reported for measuring the contractility of CMs by continuously monitoring the electrical resistance change inside a controlled incubator environment.[18,19] The devices were nicely constructed via three-dimensional (3D) printing, which required the proper design of six functional inks. The devices were proven effective for continuous, long-term measurement of CMs' contractility; however, they had a relatively low sensitivity, which is lower by 2 orders of magnitude than the devices developed in our work (see the Discussion section).

Cell drum has also been reported for measuring the contractility of CMs. Cell drum is a flexible membrane device where a thin silicone membrane is sealed on the top of a chamber.[20] Both laser sensor and pressure sensor are assembled inside the sealed chamber for monitoring membrane deflection. A positive pressure is applied through the chamber to keep the silicone membrane flat when CMs are seeded on the membrane. The stress caused by CM contraction induces a pressure change inside the chamber and causes membrane deflection, which are, respectively, detected by the pressure sensor and the laser sensor. However, the reported contractile stress of hiPSC-CMs measured by the cell drum technique is 10 times higher than the values measured with other techniques (43.1 ± 7.5 kPa vs 3.78 ± 2.09 kPa, see Table S1 and refs[19,21,22]). This may be attributed to the poor accuracy of the cell drum measurement because of the very small pressure variations caused by cell contraction, leading to a low signal-to-noise (S/N) ratio.[20,23]

Micropost arrays[24,25] and hydrogel thin films embedded with fluorescent beads (TFFB)[26−28] have been used as substrates for culturing CMs. Micropost or hydrogel film deflections caused by CM contraction are monitored via microscopy imaging and converted into forces via mechanics models. The micropost technique is able to measure contractile force, contractile velocity, and contractile power.[24,25] However, the topographical patterns of microposts trigger changes in the CMs' morphology and cytoskeletal structures, cell aggregation, and differentiation.[29] TFFB uses hydrogels and embedded fluorescent beads for measuring cell traction forces and has been employed to measure the contractile force of rat-, quail-, and human embryonic stem cell-derived CMs.[26,27] Tracking the position changes of a high number of fluorescent beads and analyzing the image data to convert the position changes into pressure fields generated by CMs are highly time-consuming.[30] Therefore, the TFFB technique reported in the literature for CM studies often focused on single-cell measurement. However, no heart cell is in isolation, and investigations on individual cells lose the

DOI: 10.1021/acsami.8b05407
ACS Appl. Mater. Interfaces 2018, 10, 21173−21183

contributions of cell-to-cell communication, gap junctions, coordinated cellular action, and vital components of heart contractile function.

In this paper, we report a microdevice array that is capable of measuring the beating rate, rhythm, and contractility of a monolayer of hiPSC-CMs. Key to this device is the integration of composites of carbon nanotubes (CNTs) and polydimethylsiloxane (PDMS), in which CM contraction causes changes in the structure of the CNT network and further the electrical resistance. hiPSC-CMs cultured on the microdevice arrays showed normal structural and physiological features, as compared to those cultured in Petri dishes in the control group. Five drugs were applied, and their effects on hiPSC-CMs were measured by the device arrays. The measured contractile stress of hiPSC-CMs ranged from 21.15 ± 0.13 to 3.96 ± 0.53 kPa under untreated and drug-treated conditions. Furthermore, because of the continuous measurement capability, the data also clearly revealed the evolution of contractile stress during the 14-day culturing period.

2. EXPERIMENTS AND METHODS

2.1. Fabrication of Device Arrays. The compositions of the device are schematically shown in Figure 1A, consisting of a glass substrate, a PDMS base structure including a suspended membrane and a microchannel, CNT stripes sandwiched within two PDMS layers, and a top PDMS layer embedded with fluorescent beads. The major steps in fabricating the CNT−PDMS device arrays are shown in Figure S1A (Supporting Information). PDMS (1:20 as the ratio of the curing agent and the PDMS polymer) was poured into a mold and baked at 80 °C for 4 h to form 16 device arrays, with each array containing 3 suspended membranes (6.35 mm in diameter and 100 μm in thickness). The baked PDMS was peeled off and cut into 16 strips, and the membranes were connected by the underlying microchannels, forming the PDMS base structure (Figure 1A). The PDMS base structure was treated by plasma and bonded to the glass slide. A hole (diameter: 0.8 mm) was formed using a biopsy punch, and a plastic tubing was connected to the underlying channels.

CNTs (diameter: 20−30 nm, length: 10−30 μm, Cheaptubes Inc. USA) and PDMS (Sylgard 184, Dow Corning) were blended with a mixing weight ratio of 1:5. CNT stripes (50 μm in thickness, 300 μm in width, and 1 cm in length) were formed on the surface of the suspended membrane by screen printing. Electrical connectors were then bonded to the glass slide using partially cured PDMS and connected to the strain sensors by using additional uncured CNT−PDMS blends, which were baked for 4 h. For verifying device membrane deflections caused by CMs' contraction through fluorescence imaging, 1:20 PDMS mixed with fluorescent beads (mean particle size: 0.5 μm; fluorescence: $\lambda_{ex} \approx$ 575 nm, $\lambda_{em} \approx$ 610 nm; Sigma) was spin-coated at a speed of 600 rpm to form a thin film on the CNT−PDMS layer. This layer is termed as the fluorescent bead layer in Figure 1A. The device was then oven baked at 80 °C for 4 h. Custom-made PDMS rings were finally bonded onto the top surface of the device array as culture chambers. Figure 1C shows a completed device array without the PDMS rings.

2.2. Calibration of CNT Sensors. The contractile stress of the hiPSC-CMs was determined according to Stoney's equation,[31] which requires the relationship between the relative resistance change ($\Delta R/R_0$) and vertical displacement (Δh) of the membrane to be established. For device calibration, a pneumatic pressure was applied using a diaphragm pump (Schwarzer, model SP 500EC) and a programmable pressure regulator (Marsh Bellofram, model 3420). The pump delivered pressure (P) into the device channels through a single inlet to bulge the suspended membrane. The height change at the center of the membrane, Δh, was measured using a zoom system (Navitar 126, Rochester, NY), and P was controlled by a custom-made LabVIEW program. Meanwhile, a constant voltage of 2.5 V was applied to each CNT sensor, and the electrical resistance signals were collected at a sampling rate of 10 Hz using an impedance spectroscope (HF2IS, Zurich Instrument). Prior to calibration, the CNT sensors were preconditioned via pneumatic straining for 24 h to ensure reproducible resistance signals. During calibration, Δh and electrical resistance (R) were recorded under different pressures.

2.3. Finite Element Analysis (FEA). FEA was conducted to characterize the vertical displacement and strain profile in the device membrane using COMSOL Multiphysics (Comsol Inc., version 5.1). The membrane had an elastic modulus of 467.5 ± 10.27 kPa (n = 6), measured by atomic force microscopy (AFM), and was modeled as an isotropic elastic material with a Poisson's ratio of 0.49. The elastic modulus of the membrane, the experimentally measured dimensions of the device structures, and the applied pressure were used in FEA. In simulation, the applied pressure was set to be 3.43 kPa, which was converted from the contractile stress of 4.5 kPa generated by a monolayer of hiPSC-CMs, as reported in ref 18. To quantify the vertical membrane displacement for different membrane thicknesses (10 to 1000 μm), the loop function in COMSOL was employed. Strain distributions in the membrane for each thickness were also obtained in simulation.

2.4. hiPSC-CMs Culturing and Contractility Measurement. hiPSC-CMs were obtained from Cellular Dynamics International. Prior to culturing, all CNT−PDMS devices were ultraviolet (UV)-sterilized. The sterilized CNT−PDMS device membranes were coated with a matrix mixture consisting of fibronectin, gelatin, and laminin and incubated at 37 °C for at least 4 h. The cells were plated at a density of 1.56×10^5 cells/cm^2 in iCell CM plating medium (Cellular Dynamics International) and cultured at 37 °C/5% CO_2. Cells were thawed in hiPSC-CMs plating medium (Cellular Dynamics International) and centrifuged for 5 min at 180g. Four hours post plating, the plating medium was replaced with iCell CM maintenance medium, and the maintenance medium was subsequently replaced every second day. The monolayer of cells was cultured for a period of 10 days. Once the hiPSC-CMs were seeded, the device array was placed in a humidified 37 °C incubator with 5% CO_2, and the electrical signal of the CNT sensors started to be recorded. A constant voltage of 2.5 V was applied to the CNT−PDMS sensors, and the sensor signals were recorded with a sampling frequency of 10 Hz. Simulation results (Figure S2D, Supporting Information) show that the potential temperature rise caused by the power consumption of CNT sensors is negligible.

2.5. Immunofluorescence Staining. The hiPSC-CMs cultured on the device array were stained and compared with the cells grown on the Petri dish. The cells were fixed after culturing for 1, 3, 5, or 10 days, washed twice with PBS, and fixed in 4% formaldehyde for 15 min at room temperature. Subsequently, the cells were washed three times with wash buffer (0.01% Triton X-100 in TBS), permeabilized with 0.1% Triton X-100 in TBS for 15 min, washed three times with wash buffer, and incubated in fresh antibody diluent solution (5% goat serum in wash buffer) for 1 h at room temperature. The cells were incubated with primary antibodies, mouse-raised anti-α-actinin diluted at 1:500, and rabbit-raised anti-MYH7 at 1:100 (both Sigma, St. Louis, USA) in antibody diluent, overnight at 4 °C, followed by Alexa Fluor 594-anti-rabbit and Alexa Fluor 594-anti-mouse secondary antibodies at 1:1000 in antibody diluent (Cell Signaling Technology, Danvers, MA) with Hoecht 33342 solution (Thermo Scientific) diluted at 1:50 000 for 1 h at room temperature, and stored in TBS prior to imaging. Images were acquired on a spinning disk confocal microscope (DMi8, Leica, German) equipped with an electron microscopy charge-coupled device (CCD) camera (C9100-13, Hamamatsu, Japan) and analyzed in ImageJ (1.8, National institutes of Health, USA).

2.6. Calcium Imaging. CMs' beating behavior is closely related to the influx of Ca^{2+}. Calcium 5 indicator (FLIPR, Molecular Devices) was employed for binding Ca^{2+} ions. Specifically, hiPSC-CMs were first loaded with a fluo-5 Ca^{2+} indicator in a medium of loading buffer [N-(2-hydroxyethyl)piperazine-N'-ethanesulfonic acid]. The cells were incubated in a humidified 37 °C incubator with 5% CO_2. Then, the cells were rewashed five times with the medium. Fluorescence was excited at 488 nm and recorded at 520 nm. Fluorescence imaging was focused on the plane of CM beating. Fluorescence videos (resolution: 512 × 384 pixels) were captured by a CCD camera (Retiga Exi,

DOI: 10.1021/acsami.8b05407
ACS Appl. Mater. Interfaces 2018, 10, 21173−21183

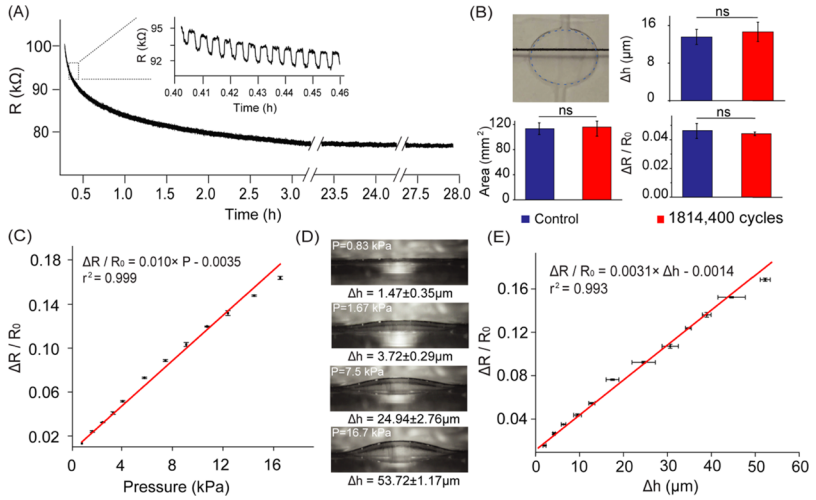

Figure 2. Device calibration. (A) Device preconditioning. Resistance signal (R) changed periodically, induced by cyclic air pressures. The mean resistance value reduced to 75 kΩ and reached equilibrium after 24 h. (B) After preconditioning, the devices underwent fatigue testing. Membrane displacement, Δh, membrane area, and $\Delta R/R_0$ before and after fatigue testing (under the actuation pressure of 3.43 kPa at 1 Hz for 21 days) did not change significantly. Measurements were made on nine device elements/membranes. (C) Calibrated relationship between the resistance change ($\Delta R/R_0$) and applied pressure. (D) Optical microscopy images of membrane deflections under different actuation pressures. (E) Calibrated relationship between $\Delta R/R_0$ and maximal vertical displacement (Δh) of the device membrane.

Qimaging) under 20× at 20 frames per second. Ca^{2+} was expressed as the intensity of fluorescence signals.

2.7. Drug Test. Five drugs (isoproterenol, verapamil, omecamtiv mecarbil (OM), ivabradine, and E-4031) from Sigma-Aldrich were tested. Drug stocks were kept at 4 °C prior to use. Drug tests were performed on hiPSC-CM monolayers during culture between days 10 and 14. Before testing each drug, 100 μL of serum-free media was added to each well of the device array, and the dose of the drug was increased gradually by adding 1 μL more drug of higher concentration each time. After each drug addition, the cells were incubated for 10 h for each dose, before CNT sensor signals were recorded to reflect the drug effect. Because the effective concentrations of each drug are different, varied concentrations were used for the five drugs.

2.8. Statistical Analysis. Each set of data was from three to six experiment repeats and are presented as values of the mean and the standard error of the mean. For differential analysis, all statistics of recorded data were processed using Student's t test with levels of 0.05 and 0.1 when they were compared to the control group. All data sets passed Shapiro–Wilk normality tests and equal variance tests. Fourier analysis was processed by Matlab (MathWorks Inc, USA). Microcal Origin 8.5 software (Microcal, Northampton, MA, USA) was used for statistical processing of data.

3. RESULTS

The use of hiPSC-CMs as vehicles for disease testing and therapy discovery is currently limited by the inability to properly measure the complex activities of the cardiac cells. We developed a platform that is capable of comprehensively measuring the beating rate, rhythm, and contractility in a monolayer of hiPSC-CMs. The CNT–PDMS device arrays are well-suited for long-term cell culturing and to monitor gradual changes of hiPSC-CMs contractility during the culturing process.

3.1. CNT–PDMS Device Characterization. *3.1.1. Device Characterization.* The thickness of the suspended PDMS membrane was measured with an optical step profiler to be 200 μm (Figure S1B, Supporting Information). The suspended membrane has two layers of PDMS sandwiching a stripe of CNT–PDMS. The thickness and width of the CNT–PDMS stripe were 50 and 150 μm, respectively. During device design, FEA (Figure S1C, Supporting Information) showed that the vertical displacement of a 500 μm-thick PDMS membrane was 14.8 μm caused by an applied stress of 4.5 kPa (contractile stress caused by a monolayer of hiPSC-CMs reported in ref 18). Under the same condition, the vertical displacement of a 200 μm-thick PDMS membrane was 32.17 μm. Therefore, we chose the 200 μm thickness in the final device design to achieve a relatively large membrane displacement and strain sensor's signal change $\Delta R/R_0$ (i.e., improved sensitivity). AFM indentation (Figure S1D, Supporting Information) was conducted, and the elastic modulus of the suspended membrane was measured to be 467.5 kPa.

3.1.2. Device Calibration. When hiPSC-CMs are cultured on the device membrane (Figure 1B), the cells exert compressive stress on the top surface of the PDMS membrane during synchronous contraction.[32,33] According to the thin film model[34] and consistent with previous observations of epithelial cells' contraction,[35] compressive stress causes the membrane to concave upwards, and the radius of curvature is determined by the magnitude of the stress exerted by hiPSC-CMs. To mimic the process and establish a calibrated relationship between the membrane displacement amplitude and CNT strain sensor's electrical resistance change, a pneumatic pressure was applied to bulge the suspended membrane. The inset in Figure 1C shows membrane bulging under the applied pressure of 16.7 kPa. To accurately measure the membrane displacement amplitude, the fluorescent beads embedded in the top PDMS layer were used for confocal microscopy imaging to measure membrane displacements (Figure 1D).

To precondition the CNT strain sensors, a sinusoidal pneumatic pressure (4 kPa, 0.1 Hz) was applied, and the corresponding periodical change of strain sensor's resistance (R) is shown in Figure 2A. The initial resistance value (R) ranged from 96.2 to 311.7 kΩ across devices. During preconditioning, the resistance change of the strain sensors decreased over time until the 24th hour. When equilibrium was reached, the resistance values of the devices (R_0) varied from 68.3 to 94.4 kΩ (Table S2 in the Supporting Information lists R and R_0 values of nine device elements before and after preconditioning). In this work, the normalized quantity, $\Delta R/R_0$, was used and

DOI: 10.1021/acsami.8b05407
ACS Appl. Mater. Interfaces 2018, 10, 21173–21183

correlated with the applied pressure (see Figures 2C and S2C in the Supporting Information) through device calibration. The sensitivity ($\Delta R/R_0$ vs pressure) of the nine device elements was experimentally determined to be 0.01 ± 0.0003 kPa^{-1}. After device preconditioning, a fatigue test was performed to evaluate potential structural degradation of the device membrane as well as CNT strain sensor's signal stability. In the 21-day fatigue test, a sinusoidal pressure (3.43 kPa,[18] 1 Hz) was applied to mimic the effect of CM beating on the device membrane, resulting in membrane deflections for 1.81×10^6 cycles. As the gas permeability of PDMS is approximately 1.0×10^3 Barrer,[36,37] for the applied pressure of 3.43 kPa, it would take 4.39×10^7 s to completely leak the compressed air through the PDMS membrane. Thus, considering the time scale of the applied pressure (1 Hz), air leakage was negligible. The same preconditioning process and fatigue tests were conducted on three independent device arrays (totally nine device elements/membranes). Before and after the fatigue tests, we measured the vertical displacement (Δh) at the center of the membrane, the area of the membrane (S), and the relative resistance change $\Delta R/R_0$ of the CNT sensor for each of the tested nine device elements/membranes. These three parameters' respective values before and after fatigue testing are 13.58 ± 1.59 μm versus 14.67 ± 2.02 μm, 113.43 ± 0.77 μm^2 versus 116.08 ± 0.38 μm^2, and (4.64 ± 0.73) × 10^{-2} versus (4.22 ± 0.98) × 10^{-2} (Figure 2B). The p values in all three cases were larger than 0.1. These results indicated no significant membrane fatigue or CNT strain sensor signal degradation after 21 days of periodic straining.

We then calibrated the relationship of the relative resistance change ($\Delta R/R_0$) of the CNT strain sensor and the vertical displacement (Δh) of the membrane. A pneumatic pressure ranging from 0 to 16.7 kPa was applied to bulge the suspended PDMS membrane. Δh was measured by microscopy imaging (Figure 2D), and the CNT resistance signal was simultaneously recorded by impedance spectroscopy. Figure S2 (Supporting Information) summarizes the calibrated membrane displacement under different actuation pressures resulting in $\Delta h = 3.37 \times P - 1.71$ ($r^2 = 0.998$). The relationship between $\Delta R/R_0$ and P was also calibrated, resulting in $\Delta R/R_0 = (0.010 \pm 0.0003) \times P - 0.0035$, ($r^2$: 0.999, n = 9 device elements), as shown in Figure 2C. From these calibration results, $\Delta R/R_0$ and Δh were quantitatively related; $\Delta R/R_0 = 0.0031 \times \Delta h - 0.0014$ (r^2 = 0.993). When hiPSC-CMs were seeded on the device membrane, the cell-generated contractile stress was determined with these calibrated relationships (Figure S2A in the Supporting Information).

3.2. Measurement of hiPSC-CMs' Physiological Structures. To assess the structure of the force-generating unit (sarcomere) and the physiological features of the hiPSC-CMs grown on the CNT−PDMS device, α-actinin staining and calcium imaging were conducted. The protein, α-actinin, is necessary for the attachment of actin filaments to the Z-lines in CMs. Immunostaining images of hiPSC-CMs grown on the PDMS−CNT device and in the Petri dish were compared. Figure 3A,B shows that α-actinin of both the groups cross-linked to actin filaments and both displayed evenly striated fibers. Sarcomere length is an indicator of the degree of overlap between the thick and thin filaments within the actin−myosin contractile apparatus of CMs. A longer sarcomere length indicates that CMs are capable of forming a larger sliding distance between the actin and myosin filaments, resulting in a higher degree of overlap and a larger contractile force. The

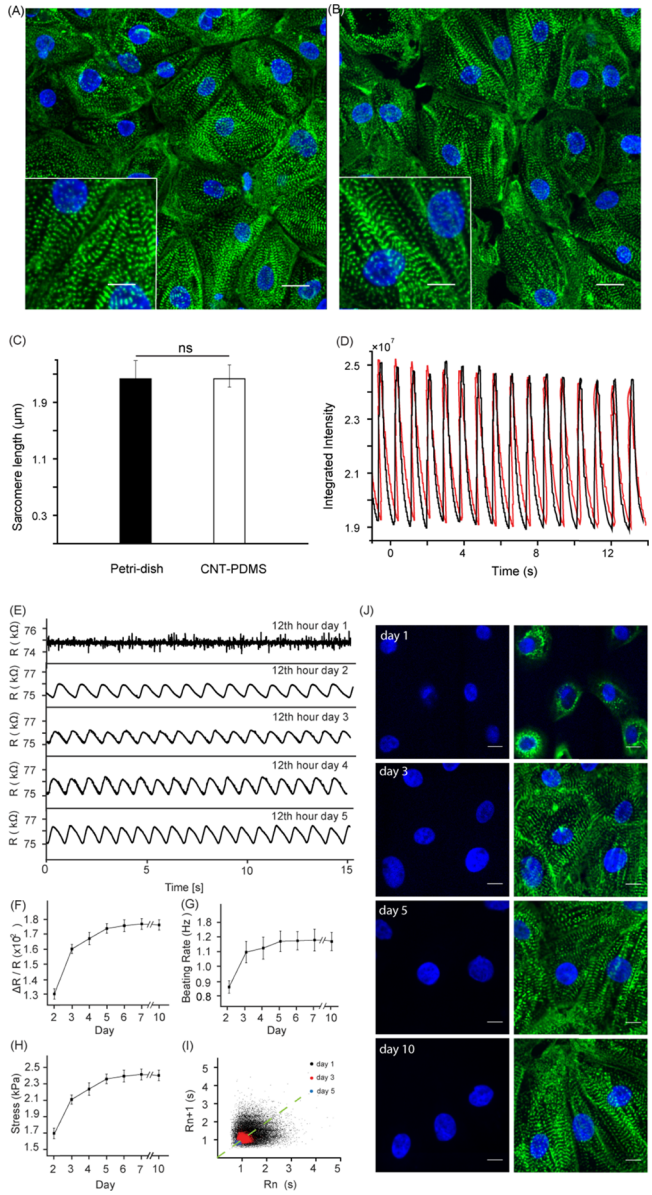

Figure 3. Evaluation of the development of hiPSC-CMs cultured on CNT−PDMS devices. Confocal images of cells cultured on a (A) Petri dish and (B) a CNT−PDMS device; the scale bar is 20 μm; the scale bar of the inset is 7.5 μm. Cells were fixed and stained: α-actinin (green) and nucleus (blue). (C) Average sarcomere length of hiPSC-CMs cultured on a Petri dish (2.25 ± 0.19 μm, n = 70) and CNT−PDMS (2.16 ± 0.13 μm, n = 70), measured on day 10. (D) Calcium transient was evaluated by the fluorescence intensity of calcium indicator fluo-5 in calcium imaging. Spontaneous calcium transients indicate that cells were electrically coupled on PDMS−CNT devices. The durations of calcium release were 0.85 ± 0.09 s on PDMS−CNT devices (black line) and 0.87 ± 0.04 s on the Petri dish (red line). (E) Measurement of CMs over the 10-day culturing process. Example CNT resistance signals from day 1 to day 5. (F) $\Delta R/R_0$, (G) beating rate, and (H) contractile stress evolution for the 10-day culture period. (I) Poincaré plot showing beating rhythm on days 1, 3, and 5. (J) α-Actinin and nuclei in fluorescence images showing the development of sarcomeres. The scale bar is 10 μm.

sarcomere length was determined by measuring the difference of gray value in neighboring α-actinins, as shown in Figure S3 (Supporting Information). Figure 3C shows that the measured sarcomere lengths in hiPSC-CMs cultured on the CNT−PDMS

DOI: 10.1021/acsami.8b05407
ACS Appl. Mater. Interfaces 2018, 10, 21173−21183

device and in the Petri dish were 2.25 ± 0.19 μm (n = 70 cells) versus 2.16 ± 0.13 μm (n = 70 cells) (p > 0.1). These results indicate the hiPSC-CMs cultured on the device membranes (Young's modulus: 467.5 ± 10.27 kPa) and those cultured in Petri dishes likely generate comparable contractile forces.

Another essential feature of CM physiology is the ability to rapidly increase the cytosolic Ca^{2+} concentration in response to spontaneous or stimulated membrane depolarization. Experimental data (Figure 3D) show that the integrated intensity of calcium released from the contracting hiPSC-CMs cultured on the CNT−PDMS device was $2.48 \times 10^7 \pm 6.27 \times 10^5$, and the value of the cells cultured on the Petri dish was $2.51 \times 10^7 \pm 4.91 \times 10^5$. In addition, the durations of calcium release were also similar (0.85 ± 0.09 s vs 0.87 ± 0.04 s, n = 7 wells, P > 0.1). The results confirmed that hiPSC-CMs cultured on the CNT−PDMS devices well preserved the cardiac contractility.

3.3. Monitoring Spontaneous Contractile Behaviors of hiPSC-CMs. After cell seeding, the device array was placed into an incubator and was connected to the impedance spectroscope, through a port on the back of the incubator, for recording the sensor signals. Figure S4A (Supporting Information) shows the dynamic sensor signal change within the first 32 h. It can be seen that the CNT sensor's resistance increased from 74.78 to 75.16 kΩ after 16 h and then fluctuated around the baseline value of 75.16 kΩ. The increase of the sensor signal in the first 16 h likely reflects the cell adhesion dynamics. Figure S4 (Supporting Information) also clearly shows the chaos state between 24 and 32 h. It is known that cells need time (typically a few hours) to have their gap junctions completely assembled[38] during the chaos state. Therefore, those cells that started to beat cannot transfer signals to their neighboring cells.

Figure 3E shows the CNT sensor signals from day 1 to day 5 (the 12th hour on each day). From day 2, regular beating of the monolayer of hiPSC-CMs began, and the beating rate and contractile stress started to increase from day 2. The sensor signal, $\Delta R/R_0$ (Figure 3F) induced by cell beating increased from $1.30 \times 10^{-2} \pm 3.50 \times 10^{-4}$ on day 2 to $1.77 \times 10^{-2} \pm 3.68 \times 10^{-4}$ on day 5 and remained largely unchanged by day 10 ($1.76 \times 10^{-2} \pm 3.52 \times 10^{-4}$). Correspondingly, the beating rate (Figure 3G) of the cells increased from 0.833 ± 0.046 Hz on day 2 and plateaued at 1.17 ± 0.068 Hz on day 5. The contractile stress (Figure 3H) increased from 1.73 ± 0.047 kPa on day 2 to 2.35 ± 0.038 kPa on day 5 and remained largely unchanged afterward (2.34 ± 0.041 kPa on day 10).

The Poincaré plot (Figure 3I), decomposed from the CNT sensor signals, reveals the beating rhythm of the cells. The beating rhythm of CMs describes the variation of the time interval between two adjacent beating periods, which can be quantitatively expressed by scatter plots known as the Poincaré plot.[39] Figure 3J shows that the distribution of scattered points on day 1 was scattered and covered a large area, indicating that cell beating was largely random. The covered area of the scattered plots decreased gradually, as shown by the red (day 3) and blue (day 5) clouds in Figure 3I, indicating that the cells' beating rhythm became more regular.

To understand the contractile stress increase over the culturing period, hiPSC-CMs were fixed at the end of day 1, day 3, day 5, and day 10 and measured by confocal imaging, where α-actinin was stained in green and nuclei were stained in blue. On day 1, immunocytochemical staining revealed that hiPSC-CMs had a small, rounded shape; there was no clear striped pattern (α-actinin); and sarcomeres were sparse. On day 3, cells became more elongated and exhibited clear striped patterns with a sarcomere length of 1.52 ± 0.11 μm. By day 5, cells displayed an organized sarcomeric structure (length: 2.14 ± 0.09 μm). Compared to day 5, cells on day 10 had a slight but an insignificant increase in the sarcomere length (2.14 ± 0.09 μm vs 2.16 ± 0.13 μm, P > 0.1). Figure S4B (Supporting Information) summarizes the sarcomere length development over the culturing process.

3.4. Drug Evaluation. We then applied the CNT−PDMS devices to measure the effect of cardiac drugs. On the molecular level, cardiac contraction follows a mechanism known as excitation−contraction coupling, which involves the formation of the action potential, the calcium-induced calcium release, and the formation of actin−myosin cross-bridges.[40] In this work, five typical clinical drugs, which are known to affect CMs' beating behaviors by regulating the excitation−contraction coupling process, were tested to demonstrate the device's effectiveness for quantitating the drug effects (Figure 4A−E). Isoproterenol, verapamil, OM, ivabradine, and E-4031, respectively, act on the β-adrenergic receptor, LTCC, myosin filament, funny channel, and hERG channel, and they affect CMs' functions by regulating contractility, beating rate, and beating rhythm.

Isoproterenol is a β-adrenergic receptor agonist. It can activate the β-adrenergic pathway, stimulate LTCCs and ryanodine receptors (RyR2) on sarcoplasmic reticulum (SR), and further cause a significant increase of the intracellular Ca^{2+} concentration.[41] Ca^{2+} binds to troponin, activates actin and myosin combination, and initiates sarcomere shortening (see solid black line in Figure 4G). As a result, isoproterenol is known to be able to increase both contractility and beating rate of CMs in a dose-dependent manner. In our experiments, four isoproterenol concentrations (0.25, 0.50, 1.00, and 2.00 μM) were tested. Each drug concentration was tested in three independent wells of hiPSC-CMs. As shown in Figure 4A, for the 2.00 μM isoproterenol group of hiPSC-CMs, compared to the control group, $\Delta R/R_0$ increased from $1.76 \times 10^{-2} \pm 7.26 \times 10^{-4}$ to $2.98 \times 10^{-2} \pm 3.97 \times 10^{-3}$. Contractile stress increased by 69.4% (2.34 ± 0.093 kPa vs 3.963 ± 0.532 kPa), and the beating rate (Figure S5 in Supporting Information) increased from 1.17 ± 0.068 to 1.33 ± 0.081 Hz (n = 3 and p < 0.05).

When CMs are depolarized by an action potential, Ca^{2+} enters the cell through the LTCC and then triggers inner Ca^{2+} release from SR, resulting in an increase of Ca^{2+} concentration in mycoplasma, a process known as "calcium-induced calcium release."[40] Verapamil is an LTCC (see Figure 4G) blocker that can decrease force generation and beating rate by inhibiting Ca^{2+} transit.[42] It has been used in the treatment of cardiovascular diseases such as hypertension and cardiac arrhythmia. Our CNT−PDMS devices quantitatively revealed the drug's effect in altering the contractile stress and beating rate of hiPSC-CM monolayers grown on the suspended membranes. The four verapamil concentrations tested in this work were 0.05, 0.10, 0.15, and 0.20 μM, and each drug concentration was tested in three independent wells of hiPSC-CMs. Figure 4B shows that the treatment of hiPSC-CMs with 0.20 μM verapamil reduced the cells' beating rate by 54.5%, from 1.12 ± 0.047 to 0.51 ± 0.069 Hz (Figure S5 in the Supporting Information). $\Delta R/R_0$ decreased from $1.76 \times 10^{-2} \pm 7.27 \times 10^{-4}$ to $8.72 \times 10^{-3} \pm 9.85 \times 10^{-4}$, and the corresponding contractile stress decreased by 50.9% from $2.34 \pm 9.31 \times 10^{-2}$ to $1.15 \pm 1.31 \times 10^{-1}$ kPa (n = 3, p < 0.05). In Figure 4F, the enlargement of the cloud size corresponding to verapamil describes the increased variability of the beating rate, whereas the shift of the cloud to the upper right corner of the plot indicates a decrease of the beating rate.

DOI: 10.1021/acsami.8b05407
ACS Appl. Mater. Interfaces 2018, 10, 21173−21183

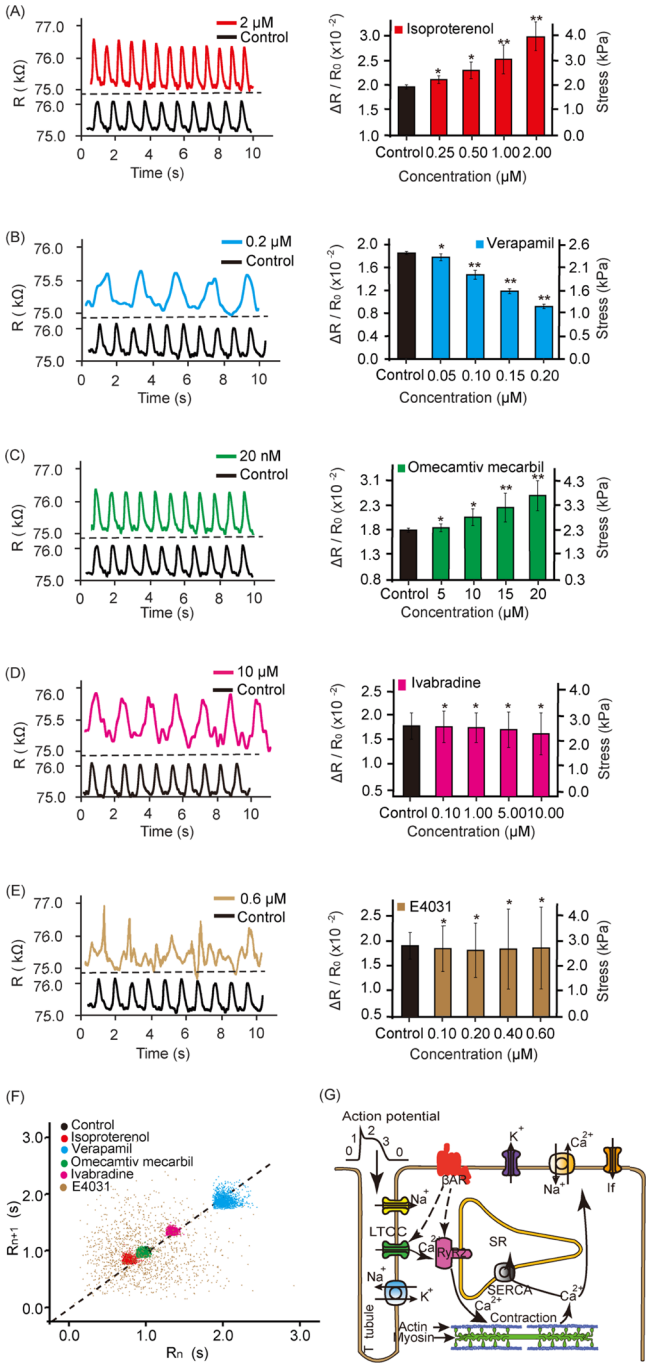

Figure 4. Platform validation with five kinds of drugs (A–E). Each drug was tested in four increasing concentrations on day 10. Data measured prior to drug treatment acted as the control group. Resistance wave and beating rhythm were plotted under maximal drug concentration and were compared to the predrug condition. Changes in $\Delta R/R_0$, contractile stress, and beating rhythm showed dose-dependent effects of five drugs on hiPSC-CM monolayers (*, $P < 0.05$; **, $P < 0.005$). (F) Poincaré plot for the beating rhythm analysis in the presence of five different drugs. (G) Mechanism of "CM excitation–contraction coupling" process. Drugs influenced the cell-beating behaviors by regulating particular receptors in this process. βAR, β-adrenergic receptor; RyR2, ryanodine receptor 2; LTCC, SERCA, sarcoplasmic/endoplasmic reticulum Ca^{2+}-ATPase.

OM is a new drug that specifically targets cardiac myosin to enhance effective actin myosin cross-bridge formation (see actin myosin cross-bridge in Figure 4G). It can activate myocardial adenosinetriphosphatase and improve energy efficiency without affecting intracellular calcium transient or the level of cyclic adenosine monophosphate.[43] Therefore, OM is able to promote contractility without increasing oxygen consumption and cardiac beating. In our experiments, four concentrations (5, 10, 15, and 20 nM) of OM were applied consecutively, and each drug concentration was tested in three independent wells of hiPSC-CMs. Figure 4C shows that 20 nM OM caused the amplitude of $\Delta R/R_0$ to increase from $1.69 \times 10^{-2} \pm 8.46 \times 10^{-4}$ to $2.98 \times 10^{-2} \pm 2.97 \times 10^{-3}$ ($n = 3$, $p < 0.05$) and caused contractile stress to increase by 76% from 2.25 ± 0.11 to 3.96 ± 0.40 kPa ($n = 3$, $p < 0.05$). However, compared with the control group, 20 nM OM only slightly increased the beating rate (Figure S5 in the Supporting Information) from 1.11 ± 0.25 to 1.13 ± 0.31 Hz ($n = 3$, $p > 0.1$).

Funny current (I_f) is an inward current that activates CMs in the hyperpolarized membrane potential phase. It plays a role in the pace-making generation and involves the formation of the spontaneous beating of hiPSC-CMss.[44] Ivabradine selectively binds to the funny channel (see I_f in Figure 4G) and inhibits the pacemaker I_f current, reducing cardiac pacemaker activity and slowing the cardiac beating without loss of contractility.[44] As shown in Figure 4D, ivabradine (0.10, 1.00, 5.00, and 10.00 μM) in our experiments led to a dose-dependent decrease of the hiPSC-CMs' beating rate (Figure S5 in the Supporting Information) from 1.16 ± 0.32 to 0.81 ± 0.30 Hz ($n = 3$, $p < 0.05$) for the concentration of 10.00 μM. Poincaré plot shows that the ivabradine cloud is located further to the top right compared with the control group, also indicating a lower beating rate. However, contractile stress only changed from 2.26 ± 0.43 to 2.00 ± 0.68 kPa ($n = 3$, $p > 0.1$) under 10.00 μM ivabradine.

The hERG channel is a K^+ channel that forms I_{Kr} current to conduct K^+ out of the CM membrane during the repolarizing phase of the cardiac action potential. E-4031 is an inhibitor of the hERG channel that affects the action potential by inhibiting I_{Kr} (see K^+ channel in Figure 4G).[45] As shown in Figure 4E, E-4031 insignificantly reduced hiPSC-CMs' contractile stress from 2.47 ± 0.48 kPa (concentration: 0.10 μM) to 2.39 ± 1.38 kPa (concentration: 0.60 μM) ($n = 3$, $p > 0.1$). With the application of 0.10 and 0.20 μM E-4031, hiPSC-CMs exhibited two spikes of beating rates. The arrhythmic beating occurred because E-4031 induces early after depolarizations (EADs), a two-step relaxation pattern in the action potential.[46] Furthermore, in the presence of 0.60 μM E-4031, CNT resistance signals showed irregular pulsing patterns, which was in accordance with the random beating rates in the Fourier analysis and the extremely large cloud area of E-4031 in the Poincaré plot (Figure 4F).

4. DISCUSSION

Strain sensors based on CNT–PDMS have been reported.[47,48] Our device represents the first CNT–PDMS platform for sensing contractility generated by CMs. In our device design, a number of considerations were accounted for. For instance, a CNT stripe was sandwiched between two PDMS layers to avoid direct CNT-cell contact and potential toxicity.[49] Furthermore, it is known that substrate stiffness can affect cellular physiology.[50,51] On substrates that have a stiffness lower than 400 kPa, sarcomere length and its shortening velocity of CMs have been shown to significantly decrease.[51,52] Because too high a substrate stiffness leads to a poor device sensitivity for measuring CMs' contractility, in this work, we used a PDMS mixing ratio of 1:20, which resulted in a substrate stiffness of 467.5 ± 10.27 kPa. With this substrate stiffness, CMs nicely formed a monolayer with

DOI: 10.1021/acsami.8b05407
ACS Appl. Mater. Interfaces 2018, 10, 21173–21183

spontaneous contractility, and their sarcomere length was comparable to the CMs grown on Petri dishes (2.25 ± 0.19 μm vs 2.16 ± 0.13 μm). Meanwhile, the CNT−PDMS devices were sufficiently sensitive to detect subtle contractility variations of CMs (e.g., caused by 5 nM OM treatment).

Our CNT−PDMS device arrays were first preconditioned by undergoing 24 h of periodic straining, after which the strain sensor signals reached equilibrium. Fatigue test was then performed to ensure reliable device performance throughout the cell culturing period of 14 days. In fatigue testing, dynamic pressure was applied for 21 days (1.81×10^6 cycles) to mimic the effect of CM beating on the suspended membrane. The results revealed that there was no significant difference in $\Delta R/R_0$ and the elastic behavior of the membrane before and after fatigue testing. On the basis of the experimentally calibrated relationship between $\Delta R/R_0$ and input pressure, the sensitivity of the device was determined to be 0.01 (kPa^{-1}). On the basis of the frequency response of the device, the bandwidth was determined to be 40 Hz (Figure S2B in Supporting Information), which is sufficient to fully capture the contractile behaviors of CMs (1−2 Hz).

AFM, TFFB, microcantilever, and cell drum are the current methods for measuring the contractile stress of CMs. Among these methods, AFM and TFFB perform measurements on single CMs. However, no cell is in isolation, and investigations of a single CM overlook the contributions of cell-to-cell communications. Cantilever and cell drum are capable of measuring the contractile stress of monolayer CMs. The reported value of contractile stress measured by cantilevers was 2−5 kPa (3.78 ± 2.09 kPa).[53] Because the cantilever method typically requires laser for measuring cantilever deflections, laser-induced heat could alter the contractile behavior of CMs. The reported contractile stress value measured by the cell drum was 43.1 ± 7.5 kPa.[20,23] Compared to the contractile stress values measured by the cantilevers and cell drum, the results from our device showed that the beating of hiPSC-CM monolayers started on day 2, plateaued on day 5, and generated an average contractile stress of 2.34 ± 0.041 kPa. This value of contractile stress is in agreement with that from cantilever measurements, but is significantly lower than the value measured by the cell drum. In cell drum, the small pressure variations (<1 Pa) caused by the contraction of CMs is challenging to be detected by the integrated pressure sensor, leading to a low S/N ratio of −9.54 dB.[23] In comparison, the S/N ratio of our device, which was experimentally determined to be 15.56 dB, is significantly higher. Furthermore, we used FEA to confirm whether yield strain occurred on our device. Yield strain determines the limits of sensing performance for the CNT−PDMS device because it represents the upper limit of contractile stress that can be applied without permanent deformation.[54] The yield strain for PDMS was varied from 0.35 to 0.55.[55] For our device, the simulated strain was 0.14 when the device membrane was bulged by the contractile stress of the cells generated on day 10 (Figure 1E). It revealed that the device deformed elastically under the contractile stress generated by a monolayer of hiPSC-CMs.

Recently, device arrays integrated with electrical strain sensors were reported.[18] The strain sensors in the 3D-printed devices were formed by thermoplastic polyurethane mixed with carbon black nanoparticles. These piezoresistive cantilevers were demonstrated to be capable of measuring contractility of CMs by continuously monitoring electrical resistance change inside a controlled incubator environment. When a monolayer of hiPSC-CMs is cultured on the piezoresistive cantilevers[18] and on our CNT−PDMS devices, the contraction of hiPSC-CMs produced an electrical resistance change ($\Delta R/R_0$) of ~1.7×10^{-4} on the piezoresistive cantilevers (see Figure 3 in ref 18) versus ~1.8×10^{-2} on our devices.

Drug testing confirmed that our PDMS−CNT devices are capable of measuring drug effects on CMs. Five types of drugs were tested, each with four different concentrations. Drug-induced changes in contractile stress, beating rate, and beating rhythm of hiPSC-CM monolayers were measured. Isoproterenol and verapamil are two isotropic drugs. In previous reports, isoproterenol was tested by cell drum,[22] micropost,[24] AFM,[56] cantilever,[11,12] and TFFB,[57] and they were used to conduct measurements on a single CM. At the concentration of 0.1−10 μM of these two drugs, the contractile stress of a single CM increased by 6−48.9% and the beating rate increased by 16.7−20%.[24,56,58] Response of monolayer CMs to these two drugs was measured by the cantilever method. Under the concentration of 10^{-3} to 1 μM, the increase of contractile stress was measured to be 2−77% and the increased beating rates were by 15−20%.[22,59] Different from these studies that measured neonatal rat CMs for drug testing, in our work, hiPSC-CMs were treated with concentrations of 0.25, 0.50, 1.00, and 2.00 μM of isoproterenol and verapamil. When the drug concentration reached 2.00 μM, the contractile stress and beating rate increased by 69.4 and 13.6%, respectively.

For verapamil testing, cell drum, cantilever, and TFFB were previously used.[22,59,60] At concentrations of 0.05−1 μM, the beating rate decreased by 23−80% and the contractile stress decreased by 19−61%. These measurements were made for a very short period of time and failed to monitor dynamic drug effects. For instance, TFFB only recorded cell behaviors for 15 s after the addition of verapamil.[46] By contrast, our device achieved continuous measurement of drug effects by capturing multiple parameters (contractile stress, beating rate, and beating rhythm). After 10 h of recording under 0.20 μM verapamil, our device generated a Poincaré plot. Over the 10 h period, the cloud size of the Poincaré plot became larger (blue scatter in Figure 4F), reflecting the side-effect of verapamil (heart arrhythmia). This effect cannot be reflected from other existing methods because of their inability to continuously measure contractile behaviors of CMs.

OM and ivabradine regulate either contractile stress or beating rate of CMs, but not both. OM is a new drug that is able to promote contractility without increasing the cardiac beating rate. Only TFFB has been used to measure the contractile response of a single hiPSC-CM with 0.1 μM OM.[61] Contractility generated by a single CM increased by 16.7%.[61] In comparison, the contractile stress of hiPSC-CM monolayers measured by our devices increased by 76% (2.25 ± 0.11 kPa vs 3.96 ± 0.40 kPa) at the drug concentration of 0.02 μM. The difference can be due to the different physiological states of hiPSC-CMs. For instance, the beating rate of hiPSC-CMs used in ref 61 was 0.64 Hz (vs 1.17 Hz of hiPSC-CMs used in our work), and the average length of sarcomere in ref 61 was 1.85 μm (vs 2.25 μm of hiPSC-CMs used in our work). A monolayer of hiPSC-CMs contains less than 1% pacemaker-like CMs, which are responsible for synchronous beating of the entire monolayer.[62] Ivabradine inhibits the funny current (I_f) of pacemaker-like CMs and reduces the beating rate of hiPSC-CM monolayers. The effect of ivabradine has been tested by a patch clamp and a microelectrode array.[63] Patch clamp and microelectrode array were used to analyze the beating rate through monitoring electrical

DOI: 10.1021/acsami.8b05407
ACS Appl. Mater. Interfaces 2018, 10, 21173−21183

impulses of CMs under different concentrations of ivabradine[63] but were unable to measure the contractile stress. Our data show that 10.00 μM ivabradine significantly reduced the beating rate of hiPSC-CM monolayers from 1.16 ± 0.32 to 0.81 ± 0.30 Hz but did not significantly alter their contractile stress (2.26 ± 0.43 vs 2.00 ± 0.68 kPa).

E-4031 is an antiarrhythmic agent. The effect of E-4031 on CMs has been measured by a patch clamp,[64] which revealed that the duration of field potential was prolonged for the concentrations of 1−30 nM, and EAD spikes appeared on field potential curves and caused cardiac arrhythmia at higher concentrations. The effect of E-4031 on contractile behaviors of CMs was measured by TFFB[46] and cantilever.[60] Neonatal rat CMs were measured for drug concentrations of 5−50 nM, and the results showed that the beating rate decreased by 30−51% and arrhythmic beating did not occur.[60] In comparison, our CNT−PDMS devices were capable of revealing large variations of contractile stress, random spikes of beating rate, and a large cloud area in Poincaré plot under the treatment of E-4031 (Figure 4E,F). Our data showed that a high concentration of E-4031 (>0.6 μM) caused arrhythmic beating of hiPSC-CMss, indicating cardiotoxicity of E-4031 at high concentrations.

5. CONCLUSIONS

This paper reported a platform that is capable of performing continuous, long-term (14 days) measurement of contractility, beating rate, and beating rhythm in a monolayer of hiPSC-CMs. The PDMS−CNT devices continuously measured the contractile stress, beating rate, and beating rhythm of hiPSC-CMs over the entire culturing process, revealing the dynamic evolution of hiPSC-CMs' contractile behaviors. Experimental data showed that cell beating started from day 2, and contractile stress plateaued by day 5. The average contractile stress generated by a monolayer of hiPSC-CMs was determined to be 2.35 ± 0.047 kPa with a beating rate of 1.17 ± 0.068. Five cardiac drugs were applied to hiPSC-CM monolayers, and the effect of each drug at different concentrations was quantified by the device arrays.

■ ASSOCIATED CONTENT

Supporting Information

The Supporting Information is available free of charge on the ACS Publications website at DOI: 10.1021/acsami.8b05407.

Schematic showing strain sensor fabrication by screen printing thin strips of CNT on PDMS, supplementary characterization of the CNT-PDMS device, statistical method of sarcomere length, CNT sensor signals in the first 32 hours of cell culturing and sarcomere length development from day 1 to day 10, beating rate response to each drug at different concentrations, summary of existing techniques for measuring the contractility of CMs, resistance of nine device elements before and after preconditioning, and CM contractile stress analysis (PDF)

■ AUTHOR INFORMATION

Corresponding Authors

*E-mail: c.simmons@utoronto.ca (C.A.S.).
*E-mail: jason.maynes@sickkids.ca (J.T.M.).
*E-mail: sun@mie.utoronto.ca (Y.S.).

ORCID

Li Wang: 0000-0002-5166-0397

Author Contributions

⊥L.W. and W.D. have contributed equally.

Notes

The authors declare no competing financial interest.

■ ACKNOWLEDGMENTS

The authors acknowledge the financial support from the Canadian Institutes of Health Research (CIHR, no. 357256) and the Natural Sciences and Engineering Research Council of Canada (NSERC) through a Collaborative Health Research Projects (CHRP) grant; from the Explore Program of CQDM and the Ontario Centres of Excellence (OCE); and from the University of Toronto via an EMHSeed grant. L.W. acknowledges a postdoctoral fellowship from Ted Rogers Centre for Heart Research Education Fund. W.D. acknowledges a China Scholarship Council scholarship (no. 201606060148). Y.S. also acknowledges the financial support from the Canada Research Chairs Program.

■ REFERENCES

(1) Mozaffarian, D.; Benjamin, E. J.; Go, A. S.; Arnett, D. K.; Blaha, M. J.; Cushman, M.; Das, S. R.; de Ferranti, S.; Després, J.-P.; Fullerton, H. J.; Howard, V. J.; Huffman, M. D.; Isasi, C. R.; Jiménez, M. C.; Judd, S. E.; Kissela, B. M.; Lichtman, J. H.; Lisabeth, L. D.; Liu, S.; MacKey, R. H.; Magid, D. J.; McGuire, D. K.; Mohler, E. R.; Moy, C. S.; Muntner, P.; Mussolino, M. E.; Nasir, K.; Neumar, R. W.; Nichol, G.; Palaniappan, L.; Pandey, D. K.; Reeves, M. J.; Rodriguez, C. J.; Rosamond, W.; Sorlie, P. D.; Stein, J.; Towfighi, A.; Turan, T. N.; Virani, S. S.; Woo, D.; Yeh, R. W.; Turner, M. B. Heart Disease and Stroke Statistics-2016 Update a Report from the American Heart Association. *Circulation* **2016**, *133*, 447.

(2) Broadley, K. J. The Langendorff Heart Preparation: Reappraisal of Its Role as a Research and Teaching Model for Coronary Vasoactive Drugs. *J. Pharmacol. Methods* **1979**, *2*, 143−156.

(3) Yu, J.; Vodyanik, M. A.; Smuga-Otto, K.; Antosiewicz-Bourget, J.; Frane, J. L.; Tian, S.; Nie, J.; Jonsdottir, G. A.; Ruotti, V.; Stewart, R.; Slukvin, I. I.; Thomson, J. A. Induced Pluripotent Stem Cell Lines Derived from Human Somatic Cells. *Science* **2007**, *318*, 1917−1920.

(4) Bieling, P.; Li, T.-D.; Weichsel, J.; McGorty, R.; Jreij, P.; Huang, B.; Fletcher, D. A.; Mullins, R. D. Force Feedback Controls Motor Activity and Mechanical Properties of Self-Assembling Branched Actin Networks. *Cell* **2016**, *164*, 115−127.

(5) Garofalo, F.; Pellegrino, D.; Amelio, D.; Tota, B. The Antarctic Hemoglobinless Icefish, Fifty Five Years Later: A Unique Cardiocirculatory Interplay of Disaptation and Phenotypic Plasticity. *Comp. Biochem. Physiol., Part A: Mol. Integr. Physiol.* **2009**, *154*, 10−28.

(6) Pieske, B.; Kretschmann, B.; Meyer, M.; Holubarsch, C.; Weirich, J.; Posival, H.; Minami, K.; Just, H.; Hasenfuss, G. Alterations in Intracellular Calcium Handling Associated With the Inverse Force-Frequency Relation in Human Dilated Cardiomyopathy. *Circulation* **1995**, *92*, 1169−1178.

(7) Fu, Y.; Westenbroek, R. E.; Scheuer, T.; Catterall, W. A. Basal and β-Adrenergic Regulation of the Cardiac Calcium Channel CaV1.2 Requires Phosphorylation of Serine 1700. *Proc. Natl. Acad. Sci. U.S.A.* **2014**, *111*, 16598−16603.

(8) Giaever, I.; Keese, C. R. Monitoring Fibroblast Behavior in Tissue Culture with an Applied Electric Field. *Proc. Natl. Acad. Sci. U.S.A.* **1984**, *81*, 3761−3764.

(9) Xiao, L.; Hu, Z.; Zhang, W.; Wu, C.; Yu, H.; Wang, P. Evaluation of Doxorubicin Toxicity on Cardiomyocytes Using a Dual Functional Extracellular Biochip. *Biosens. Bioelectron.* **2010**, *26*, 1493−1499.

(10) Qian, F.; Huang, C.; Lin, Y.-D.; Ivanovskaya, A. N.; O'Hara, T. J.; Booth, R. H.; Creek, C. J.; Enright, H. A.; Soscia, D. A.; Belle, A. M.; Liao, R.; Lightstone, F. C.; Kulp, K. S.; Wheeler, E. K. Simultaneous Electrical Recording of Cardiac Electrophysiology and Contraction on Chip. *Lab Chip* **2017**, *17*, 1732−1739.

DOI: 10.1021/acsami.8b05407
ACS Appl. Mater. Interfaces 2018, 10, 21173−21183

(11) Park, J.; Ryu, J.; Choi, S. K.; Seo, E.; Cha, J. M.; Ryu, S.; Kim, J.; Kim, B.; Lee, S. H. Real-Time Measurement of the Contractile Forces of Self-Organized Cardiomyocytes on Hybrid Biopolymer Microcantilevers. *Anal. Chem.* **2005**, *77*, 6571−6580.
(12) Kim, J. Y.; Choi, Y.-S.; Lee, B.-K.; Lee, D.-W. Surface-Patterned SU-8 Cantilever Arrays for Preliminary Screening of Cardiac Toxicity. *Biosens. Bioelectron.* **2016**, *80*, 456−462.
(13) van Breugel, H. H. F. I.; Bär, P. R. D. Power Density and Exposure Time of He-Ne Laser Irradiation Are More Important Than Total Energy Dose in Photo-Biomodulation of Human Fibroblasts in vitro. *Laser Surg. Med.* **1992**, *12*, 528−537.
(14) Shen, S.; Henry, A.; Tong, J.; Zheng, R.; Chen, G. Polyethylene Nanofibres with Very High Thermal Conductivities. *Nat. Nanotechnol.* **2010**, *5*, 251−255.
(15) Wang, Q.-F.; Shen, W.-L.; Liu, C.; Mu, D.-L.; Wu, X.-F.; Guo, N.-G.; Zhu, J.-Q. Effects of Multi-Environmental Factors on Physiological and Biochemical Responses of Large Yellow Croaker, Larimichthys Crocea. *Chemosphere* **2017**, *184*, 907−915.
(16) Chung, J.-H.; Biesiadecki, B. J.; Ziolo, M. T.; Davis, J. P.; Janssen, P. M. L. Myofilament Calcium Sensitivity: Role in Regulation of in Vivo Cardiac Contraction and Relaxation. *Front. Physiol.* **2016**, *7*, 562.
(17) Gilchrist, K. H.; Giovangrandi, L.; Whittington, R. H.; Kovacs, G. T. A. Sensitivity of Cell-Based Biosensors to Environmental Variables. *Biosens. Bioelectron.* **2005**, *20*, 1397−1406.
(18) Lind, J. U.; Busbee, T. A.; Valentine, A. D.; Pasqualini, F. S.; Yuan, H.; Yadid, M.; Park, S.-J.; Kotikian, A.; Nesmith, A. P.; Campbell, P. H.; Vlassak, J. J.; Lewis, J. A.; Parker, K. K. Instrumented Cardiac Microphysiological Devices via Multimaterial Three-Dimensional Printing. *Nat. Mater.* **2016**, *16*, 303−308.
(19) Matsudaira, K.; Nguyen, T.-V.; Shoji, K. H.; Tsukagoshi, T.; Takahata, T.; Shimoyama, I. MEMS Piezoresistive Cantilever for the Direct Measurement of Cardiomyocyte Contractile Force. *J. Micromech. Microeng.* **2017**, *27*, 105005.
(20) Trzewik, J.; Artmann-Temiz, A.; Linder, P. T.; Demirci, T.; Digel, I.; Artmann, G. M. Evaluation of Lateral Mechanical Tension in Thin-Film Tissue Constructs. *Ann. Biomed. Eng.* **2004**, *32*, 1243−1251.
(21) Polacheck, W. J.; Chen, C. S. Measuring Cell-Generated Forces: A Guide to the Available Tools. *Nat. Methods* **2016**, *13*, 415−423.
(22) Goßmann, M.; Frotscher, R.; Linder, P.; Neumann, S.; Bayer, R.; Epple, M.; Staat, M.; Artmann, A.; Artmann, G. M. Mechano-Pharmacological Characterization of Cardiomyocytes Derived from Human Induced Pluripotent Stem Cells. *Cell. Physiol. Biochem.* **2016**, *38*, 1182−1198.
(23) Linder, P.; Trzewik, J.; Rüffer, M.; Artmann, G. M.; Digel, I.; Kurz, R.; Rothermel, A.; Robitzki, A.; Artmann, A. T. Contractile Tension and Beating Rates of Self-Exciting Monolayers and 3D-Tissue Constructs of Neonatal Rat Cardiomyocytes. *Med. Biol. Eng. Comput.* **2010**, *48*, 59−65.
(24) Beussman, K. M.; Rodriguez, M. L.; Leonard, A.; Taparia, N.; Thompson, C. R.; Sniadecki, N. J. Micropost Arrays for Measuring Stem Cell-Derived Cardiomyocyte Contractility. *Methods* **2016**, *94*, 43−50.
(25) Han, S. J.; Bielawski, K. S.; Ting, L. H.; Rodriguez, M. L.; Sniadecki, N. J. Decoupling Substrate Stiffness, Spread Area, and Micropost Density: A Close Spatial Relationship between Traction Forces and Focal Adhesions. *Biophys. J.* **2012**, *103*, 640−648.
(26) Plotnikov, S. V.; Sabass, B.; Schwarz, U. S.; Waterman, C. M. *High-resolution Traction Force Microscopy*, 1st ed.; Elsevier Inc., 2014; Vol. *123*.
(27) Munevar, S.; Wang, Y.-l.; Dembo, M. Traction Force Microscopy of Migrating Normal and H-Ras Transformed 3T3 Fibroblasts. *Biophys. J.* **2001**, *80*, 1744−1757.
(28) Mierke, C. T.; Rosel, D.; Fabry, B.; Brabek, J. Contractile Forces in Tumor Cell Migration. *Eur. J. Cell Biol.* **2008**, *87*, 669−676.
(29) Wu, Y.-N.; Law, J. B. K.; He, A. Y.; Low, H. Y.; Hui, J. H. P.; Lim, C. T.; Yang, Z.; Lee, E. H. Substrate Topography Determines the Fate of Chondrogenesis from Human Mesenchymal Stem Cells Resulting in Specific Cartilage Phenotype Formation. *Nanomed. Nanotechnol. Biol. Med.* **2014**, *10*, 1507−1516.
(30) del Álamo, J. C.; Lemons, D.; Serrano, R.; Savchenko, A.; Cerignoli, F.; Bodmer, R.; Mercola, M. High Throughput Physiological Screening of iPSC-Derived Cardiomyocytes for Drug Development. *Biochim. Biophys. Acta, Mol. Cell Res.* **2016**, *1863*, 1717−1727.
(31) Klein, C. A. How Accurate Are Stoney's Equation and Recent Modifications. *J. Appl. Phys.* **2000**, *88*, 5487−5489.
(32) Nguyen, T. K.; Lee, D.-W.; Lee, B.-K. Numerical Investigation of Perforated Polymer Microcantilever Sensor for Contractile Behavior of Cardiomyocytes. *Jpn. J. Appl. Phys.* **2017**, *56*, 06GM01.
(33) Liu, X.; Zhao, H.; Lu, Y.; Li, S.; Lin, L.; Du, Y.; Wang, X. In Vitro Cardiomyocyte-Driven Biogenerator Based on Aligned Piezoelectric Nanofibers. *Nanoscale* **2016**, *8*, 7278−7286.
(34) Spaepen, F. Interfaces and Stresses in Thin Films. *Acta Mater.* **2000**, *48*, 31−42.
(35) Miquelard-Garnier, G.; Zimberlin, J. A.; Sikora, C. B.; Wadsworth, P.; Crosby, A. Polymer Microlenses for Quantifying Cell Sheet Mechanics. *Soft Matter* **2010**, *6*, 398.
(36) Merkel, T. C.; Bondar, V. I.; Nagai, K.; Freeman, B. D.; Pinnau, I. Gas Sorption, Diffusion, and Permeation in Poly(dimethylsiloxane). *J. Polym. Sci., Part B: Polym. Phys.* **2000**, *38*, 415−434.
(37) Firpo, G.; Angeli, E.; Repetto, L.; Valbusa, U. Permeability Thickness Dependence of Polydimethylsiloxane (PDMS) Membranes. *J. Membr. Sci.* **2015**, *481*, 1−8.
(38) Gaietta, G. Multicolor and Electron Microscopic Imaging of Connexin Trafficking. *Science* **2002**, *296*, 503−507.
(39) Huikuri, H. V.; Seppänen, T.; Koistinen, M. J.; Airaksinen, K. E. J.; Ikäheimo, M. J.; Castellanos, A.; Myerburg, R. J. Abnormalities in Beat-to-Beat Dynamics of Heart Rate before the Spontaneous Onset of Life-Threatening Ventricular Tachyarrhythmias in Patients with Prior Myocardial Infarction. *Circulation* **1996**, *93*, 1836−1844.
(40) Bers, D. M. Cardiac Excitation−Contraction Coupling. *Nature* **2002**, *415*, 198−205.
(41) Lymperopoulos, A.; Rengo, G.; Koch, W. J. Adrenergic Nervous System in Heart Failure: Pathophysiology and Therapy. *Circ. Res.* **2013**, *113*, 739−753.
(42) Tanaka, T.; Tohyama, S.; Murata, M.; Nomura, F.; Kaneko, T.; Chen, H.; Hattori, F.; Egashira, T.; Seki, T.; Ohno, Y.; Koshimizu, U.; Yuasa, S.; Ogawa, S.; Yamanaka, S.; Yasuda, K.; Fukuda, K. In Vitro Pharmacologic Testing Using Human Induced Pluripotent Stem Cell-Derived Cardiomyocytes. *Biochem. Biophys. Res. Commun.* **2009**, *385*, 497−502.
(43) Liu, L. C. Y.; Dorhout, B.; van der Meer, P.; Teerlink, J. R.; Voors, A. A. Omecamtiv Mecarbil: A New Cardiac Myosin Activator for the Treatment of Heart Failure. *Expert Opin. Invest. Drugs* **2015**, *25*, 117−127.
(44) Casini, S.; Verkerk, A. O.; Remme, C. A. Human iPSC-Derived Cardiomyocytes for Investigation of Disease Mechanisms and Therapeutic Strategies in Inherited Arrhythmia Syndromes: Strengths and Limitations. *Cardiovasc. Drugs Ther.* **2017**, *31*, 325−344.
(45) Matsuo, J.; Nakamura, Y.; Izumi-Nakaseko, H.; Ando, K.; Sekino, Y.; Sugiyama, A. Possible Effects of Inhibition of IKr and IKs on Field-Potential Waveforms in the Human iPS Cell-Derived Cardiomyocytes Sheet. *J. Pharmacol. Sci.* **2015**, *128*, 92−95.
(46) Hayakawa, T.; Kunihiro, T.; Ando, T.; Kobayashi, S.; Matsui, E.; Yada, H.; Kanda, Y.; Kurokawa, J.; Furukawa, T. Image-Based Evaluation of Contraction-Relaxation Kinetics of Human-Induced Pluripotent Stem Cell-Derived Cardiomyocytes: Correlation and Complementarity with Extracellular Electrophysiology. *J. Mol. Cell. Cardiol.* **2014**, *77*, 178−191.
(47) So, H.-M.; Sim, J. W.; Kwon, J.; Yun, J.; Baik, S.; Chang, W. S. Carbon Nanotube Based Pressure Sensor for Flexible Electronics. *Mater. Res. Bull.* **2013**, *48*, 5036−5039.
(48) Cai, L.; Song, L.; Luan, P.; Zhang, Q.; Zhang, N.; Gao, Q.; Zhao, D.; Zhang, X.; Tu, M.; Yang, F.; Zhou, W.; Fan, Q.; Luo, J.; Zhou, W.; Ajayan, P. M.; Xie, S. Super-Stretchable, Transparent Carbon Nanotube-Based Capacitive Strain Sensors for Human Motion Detection. *Sci. Rep.* **2013**, *3*, 3048.
(49) Ladeira, M. S.; Andrade, V. A.; Gomes, E. R. M.; Aguiar, C. J.; Moraes, E. R.; Soares, J. S.; Silva, E. E.; Lacerda, R. G.; Ladeira, L. O.;

DOI: 10.1021/acsami.8b05407
ACS Appl. Mater. Interfaces 2018, 10, 21173−21183

Jorio, A.; Lima, P.; Leite, M. F.; Resende, R. R.; Guatimosim, S. Highly Efficient siRNA Delivery System into Human and Murine Cells Using Single-Wall Carbon Nanotubes. *Nanotechnology* **2010**, *21*, 385101.
(50) Hazeltine, L. B.; Simmons, C. S.; Salick, M. R.; Lian, X.; Badur, M. G.; Han, W.; Delgado, S. M.; Wakatsuki, T.; Crone, W. C.; Pruitt, B. L.; Palecek, S. P. Effects of Substrate Mechanics on Contractility of Cardiomyocytes Generated from Human Pluripotent Stem Cells. *Int. J. Cell Biol.* **2012**, *2012*, 1−13.
(51) Hersch, N.; Wolters, B.; Dreissen, G.; Springer, R.; Kirchgeßner, N.; Merkel, R.; Hoffmann, B. The Constant Beat: Cardiomyocytes Adapt Their Forces by Equal Contraction upon Environmental Stiffening. *Biol. Open* **2013**, *2*, 351−361.
(52) Broughton, K. M.; Russell, B. Cardiomyocyte Subdomain Contractility Arising from Microenvironmental Stiffness and Topography. *Biomech. Model. Mechanobiol.* **2015**, *14*, 589−602.
(53) Rajagopalan, J.; Taher, M.; Saif, A. MEMS Sensors and Microsystems for Cell Mechanobiology. *J. Micromech. Microeng.* **2011**, *21*, 054002.
(54) Mordina, B.; Tiwari, R. K.; Setua, D. K.; Sharma, A. Superior Elastomeric Nanocomposites with Electrospun Nanofibers and Nanoparticles of CoFe2O4 for Magnetorheological Applications. *RSC Adv.* **2015**, *5*, 19091−19105.
(55) Pimentel, D. M.; de Oliveira, F. M.; dos Santos, W. T. P.; Kubota, L. T.; Damos, F. S.; Luz, R. C. S. Development of a Selective and Sensitive Sensor for Urate Determination Based on Tris(1,10-phenantroline)copper(II) Bis(tetracyanoquinodimethanide) Adsorbed on Carbon Nanotubes. *J. Braz. Chem. Soc.* **2015**, *26*, 2035−2045.
(56) Pesl, M.; Pribyl, J.; Acimovic, I.; Vilotic, A.; Jelinkova, S.; Salykin, A.; Lacampagne, A.; Dvorak, P.; Meli, A. C.; Skladal, P.; Rotrekl, V. Atomic Force Microscopy Combined with Human Pluripotent Stem Cell Derived Cardiomyocytes for Biomechanical Sensing. *Biosens. Bioelectron.* **2016**, *85*, 751−757.
(57) Huebsch, N.; Loskill, P.; Deveshwar, N.; Spencer, C. I.; Judge, L. M.; Mandegar, M. A.; Fox, C. B.; Mohamed, T. M. A.; Ma, Z.; Mathur, A.; Sheehan, A. M.; Truong, A.; Saxton, M.; Yoo, J.; Srivastava, D.; Desai, T. A.; So, P.-L.; Healy, K. E.; Conklin, B. R. Miniaturized iPS-Cell-Derived Cardiac Muscles for Physiologically Relevant Drug Response Analyses. *Sci. Rep.* **2016**, *6*, 24726.
(58) Huebsch, N.; Loskill, P.; Deveshwar, N.; Spencer, C. I.; Judge, L. M.; Mandegar, M. A.; Fox, C. B.; Mohamed, T. M. A.; Ma, Z.; Mathur, A.; Sheehan, A. M.; Truong, A.; Saxton, M.; Yoo, J.; Srivastava, D.; Desai, T. A.; So, P.-L.; Healy, K. E.; Conklin, B. R. Miniaturized iPS-Cell-Derived Cardiac Muscles for Physiologically Relevant Drug Response Analyses. *Sci. Rep.* **2016**, *6*, 24726.
(59) Gaitas, A.; Malhotra, R.; Li, T.; Herron, T.; Jalife, J. A Device for Rapid and Quantitative Measurement of Cardiac Myocyte Contractility. *Rev. Sci. Instrum.* **2015**, *86*, 034302.
(60) Dai, Y.; Oyunbaatar, N.-E.; Lee, B.-K.; Kim, E.-S.; Lee, D.-W. Spiral-Shaped SU-8 Cantilevers for Monitoring Mechanical Response of Cardiomyocytes Treated with Cardiac Drugs. *Sens. Actuators, B* **2018**, *255*, 3391.
(61) Ribeiro, A. J. S.; Schwab, O.; Mandegar, M. A.; Ang, Y.-S.; Conklin, B. R.; Srivastava, D.; Pruitt, B. L. Multi-Imaging Method to Assay the Contractile Mechanical Output of Micropatterned Human iPSC-Derived Cardiac Myocytes. *Circ. Res.* **2017**, *120*, 1572−1583.
(62) Devalla, H. D.; Schwach, V.; Ford, J. W.; Milnes, J. T.; El-Haou, S.; Jackson, C.; Gkatzis, K.; Elliott, D. A.; de Sousa Lopes, S. M. C.; Mummery, C. L.; Verkerk, A. O.; Passier, R. Atrial-like Cardiomyocytes from Human Pluripotent Stem Cells Are a Robust Preclinical Model for Assessing Atrial-Selective Pharmacology. *EMBO Mol. Med.* **2015**, *7*, 394−410.
(63) You, J.; Moon, H.; Lee, B. Y.; Jin, J. Y.; Chang, Z. E.; Kim, S. Y.; Park, J.; Hwang, Y.-S.; Kim, J. Cardiomyocyte Sensor Responsive to Changes in Physical and Chemical Environments. *J. Biomech.* **2014**, *47*, 400−409.
(64) Nakamura, Y.; Matsuo, J.; Miyamoto, N.; Ojima, A.; Ando, K.; Kanda, Y.; Sawada, K.; Sugiyama, A.; Sekino, Y. Assessment of Testing Methods for Drug-Induced Repolarization Delay and Arrhythmias in an iPS Cell−Derived Cardiomyocyte Sheet: Multi-Site Validation Study. *J. Pharmacol. Sci.* **2014**, *124*, 494−501.

DOI: 10.1021/acsami.8b05407
ACS Appl. Mater. Interfaces 2018, 10, 21173−21183